15

Ion Cyclotron Waves in the Solar Wind

H. Y. Wei,[1] L. K. Jian,[2] C. T. Russell,[1] and N. Omidi[3]

15.1. INTRODUCTION

The ion cyclotron waves (ICWs) we discuss in this chapter refer to electromagnetic transverse waves with nearly field-aligned propagation, circular polarization, and frequencies near the proton gyro-frequency. Such waves are frequently observed in the solar wind during the interactions between the magnetized solar wind plasma and the freshly created ions from the exospheres of comets or planets [e.g., see Chapter 20 of this volume], or in the magnetospheres of Jupiter and Saturn during the interactions between mass-loading from their moons (e.g., Io and Enceladus) and the magnetospheric plasma [e.g., see Chapter 21 of this volume]. These waves can be generated from the free energy of ion species with highly anisotropic temperature distributions in which the temperature perpendicular to the magnetic field is much higher than that parallel to the field. ICWs have been used as diagnostic tools for estimating the mass-loading sources and rates. However, the ICW studies we review in this chapter are different. They are not due to either the solar wind–exosphere interaction or the magnetosphere–moon interaction, but they are observed in the solar wind over a wide range of heliocentric distances, at all solar longitudes, and at locations far from planets or comets.

[1] *Department of Earth, Planetary and Space Sciences, University of California, Los Angeles, California, USA*

[2] *Department of Astronomy, University of Maryland, College Park, Maryland, USA*

[3] *Solana Scientific Inc., Solana Beach, California, USA*

15.2. ICWS OBSERVED IN THE SOLAR WIND AT 1 AU

An example of the ICWs detected by the STEREO-A spacecraft is shown in Figure 15.1 [*Jian et al*., 2009]. This event was observed on July 31, 2007, when the spacecraft was at 0.96 AU and 13° away from the Earth. The time series of the magnetic field components and strength are shown in the radial-tangential-normal (RTN) coordinates, where R points away from the Sun to the spacecraft, T is formed by the cross product of the solar rotation axis and R and lies in the solar equatorial plane, and N completes a right-hand coordinate system and is the projection of the solar rotational axis in the plane of the sky. The left panel shows a sinusoidal wave form lasting more than 3 min, and the right panel shows significant enhancement near 0.3 Hz in the transverse power, which is also much stronger than the compressional power. The compressional power is calculated from the Fourier transform of the field magnitude, B, and the transverse power is calculated by summing powers of B_R, B_T, and B_N and subtracting the power of the field magnitude, all in units of nT^2/Hz. In the spacecraft frame ($f_{s/c}$), the wave frequency at the peak transverse power is above the local proton gyro-frequency (f_{pc}), which is 0.076 Hz. The f_{pc} shown in Figure 15.1 is Doppler-shifted to the spacecraft frame, using the relationship in *Jian et al*. [2009] as is described later in this section. Wave analysis in the interval T1–T2 using the *Means* [1972] method gives a wave ellipticity of −0.95 and a wave propagation angle of 1.2° from the magnetic field. This wave analysis method uses the quadrature power spectral matrix, and the sign of ellipticity tells the left-handed (negative sign) and right-handed (positive sign) polarizations of the wave [*Means*, 1972]. One way to visualize the wave handedness is to project the trajectory

Low-Frequency Waves in Space Plasmas, Geophysical Monograph 216, First Edition.
Edited by Andreas Keiling, Dong-Hun Lee, and Valery Nakariakov.

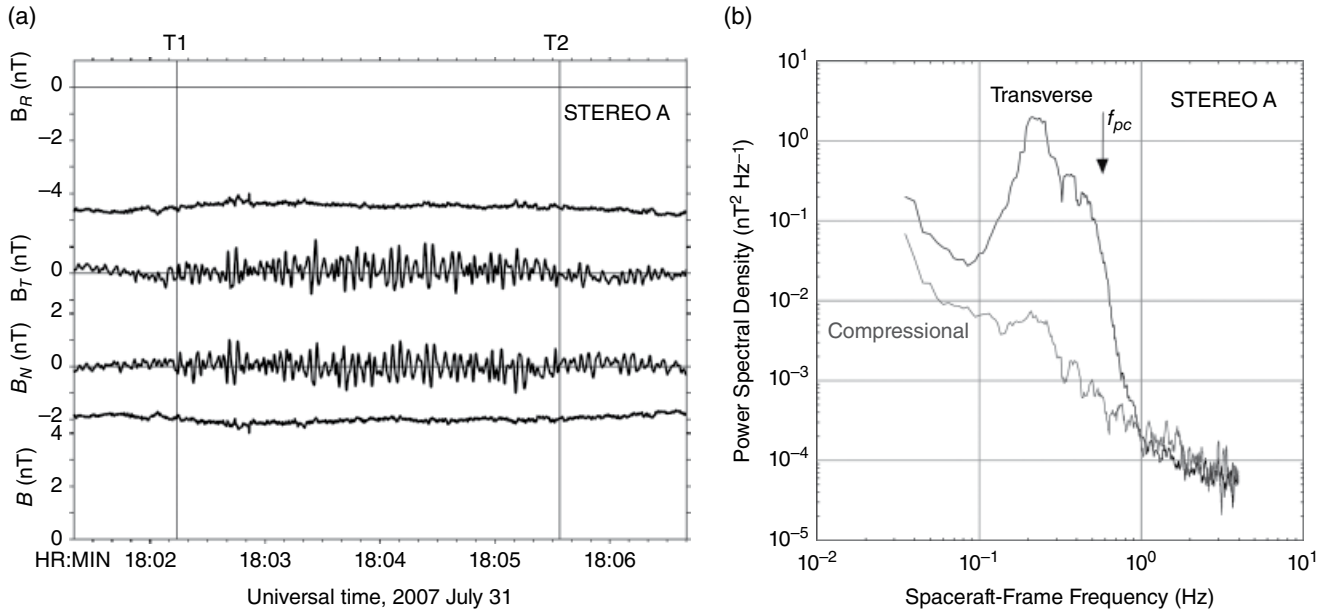

Figure 15.1 ICW as seen from the STEREO A spacecraft in the RTN coordinates: (a) 8 Hz magnetic field vector; (b) power spectrum of the wave during the interval T1–T2 marked in (a) smoothed in frequency using 13 frequency band averaging [*Jian et al.,* 2009].

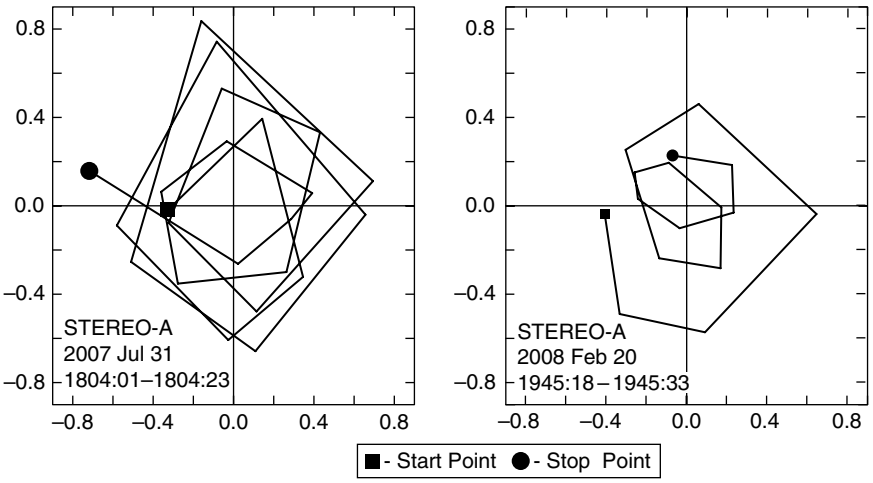

Figure 15.2 Hodograms of two LH and RH waves. The background magnetic field is perpendicular to the plane pointing outward.

of the tip of the wave magnetic field vector versus time in the plane perpendicular to the wave vector, which is called a hodogram. The left panel of Figure 15.2 shows the hodogram of these waves, with the wave rotating in a left-handed sense about the magnetic field. There are also many right-handed polarized waves observed in the spacecraft frame, whose other wave properties are very similar to the left-handed polarized ICWs [*Jian et al.*, 2009, 2010]. The right panel of Figure 15.2 shows an example of a right-handed polarized ICW.

These waves are in fact identical, except that the waves have been significantly Doppler-shifted by the solar wind flow. In the observer's frame (i.e., the spacecraft frame), the wave frequency is Doppler-shifted as, $f_{s/c} = f_{sw} + \dfrac{\vec{k}\cdot\vec{V}_{sw}}{2\pi} = f_{sw}\left(1+\dfrac{V_{sw}}{V_{ph}}\hat{k}\cdot\hat{V}_{sw}\right)$, where $\vec{k}$ is the wave vector, $\vec{V}_{sw}$ is the solar wind velocity relative to the spacecraft, f_{sw} and $f_{s/c}$ are the wave frequencies in the solar wind frame and the spacecraft frame, and V_{ph} is the phase speed of the wave. In the solar wind frame, the phase speed of the ICW can usually be approximated as the local Alfvén speed. For the example in Figure 15.1, if $\hat{k}\cdot\hat{V}_{sw}$ is positive (i.e., for waves propagating away from the Sun),

the wave frequency from the spacecraft frame to the solar wind frame is Doppler-shifted to a lower frequency, which is equivalent to the local proton gyro-frequency (i.e., 0.076 Hz) to be Doppler-shifted to a higher frequency from the solar wind frame to the spacecraft frame. Thus the Doppler-shifted proton gyro-frequency marked in Figure 15.1 is above the peak frequency of the wave in the spacecraft frame. *Jian et al*. [2009] argued that this condition (i.e., the wave frequency being smaller than proton gyro-frequency in the solar wind frame) is required so that the wave has not been damped strongly by the solar wind thermal protons if it has a frequency far below f_{pc} in the plasma frame (i.e., the solar wind frame). Because the solar wind is super-Alfvénic at 1 AU, the Doppler-shift term $\left(\frac{\vec{k} \cdot \vec{V}_{sw}}{2\pi} \approx \frac{V_{sw}}{V_A} \hat{k} \cdot \hat{V}_{sw} \right)$ in the equation is usually much larger than the other term f_{sw} during the wave intervals that usually have the magnetic field mostly in the radial direction, which means that a left-handed wave in the solar wind frame is Doppler-shifted to a higher frequency in the spacecraft frame if $\hat{k} \cdot \hat{V}_{sw}$ is positive. However, if $\hat{k} \cdot \hat{V}_{sw}$ is negative, the wave frequency is Doppler-shifted to negative values, which means the wave becomes a right-handed wave in the spacecraft frame. So, even though there are both left-handed (LH) and right-handed (RH) waves in the spacecraft frame, they could both be left-handed polarized in the solar wind frame. Thus these waves are interpreted to be ICWs, since their other wave properties are consistent with ICWs [*Jian et al*., 2009].

A statistical study of such ICWs was performed by *Jian et al*. [2009] with 246 events from STEREO-A (July 26–August 2, 2007) and STEREO-B (July 25–August 1, 2007) data. Thirty-six percent of these events were observed as RH and 64% as LH waves in the spacecraft frame, but they were all LH in the solar wind frame after correcting for the Doppler shift. Figure 15.3 compares the properties for LH and RH waves in the spacecraft frame. The wave power is stronger for LH waves than for RH waves, with a median transverse power of 0.02 and 0.004 nT^2/Hz, respectively. Other wave properties are similar between LH and RH waves, with the LH waves having slightly smaller propagation angles and higher frequency in the spacecraft frame. *Jian et al*. [2009, 2010, 2014] also compared the solar wind parameters for the periods with and without wave occurrence. The largest difference is that the interplanetary magnetic field orientation is more radial when the waves are present than when they are absent. The authors attribute the enhanced wave occurrence rate during radial magnetic field geometry to the minimal damping effect under such conditions. The waves are expected to be Landau damped when they propagate at a finite angle to the magnetic field. For nonradial field geometry, the wave propagation angle gets larger with distance from the source region; thus the wave suffers severe damping. As the wave is carried outward, the index of refraction changes, so the wave normal is bent into a more radial direction and away from the magnetic fields, allowing greater damping. When the field is more radial, the refraction and damping are less effective [*Jian et al*., 2009].

15.3. ICW STORMS AT 1 AU

The duration of the wave storms can last from tens of seconds to over an hour. *Jian et al*. [2014] named the events lasting continuously for over 10 min as low-frequency wave storms, and performed comprehensive studies on them. The storm events are often accompanied with short-duration events with time separations of a few minutes. There were 241 storm events detected by STEREO-A in 2008, which occurred cumulatively 0.9% of the time. The characteristics of waves are similar whether they occur as storms or in short-duration isolated wave packets. The wave frequency in the spacecraft frame has an average value of 0.178 ± 0.005 Hz and a median value of 0.169 Hz, which are about three times the local proton gyro-frequency. The ICMEs, interplanetary shocks, close encounters of comets, solar flares, and energetic particle events were checked to determine if the waves could be associated with the disturbances in the solar wind. *Jian et al*. [2014] found that among the 241 storm events, only two storm events were observed within half an hour of the shocks, and that a small fraction of the storm events occurred during solar energetic proton events when the three-hour average of 1.8–3.6 MeV proton rate exceeded 5×10^{-4} cm^{-2}sr^{-1}s^{-1}MeV^{-1}. The majority of these storm events are not associated with any ICMEs, shocks, flares, or solar energetic particle events, thus excluding them as wave generation sources. Sources in the pickup of planetary and cometary atmospheres are also unlikely because the majority of the wave events are far away from them.

To better understand the wave generation conditions, the solar wind parameters were compared during wave-storm periods and during the whole period of year 2008, shown in Figure 15.4. The left column shows histograms of the distribution of solar wind parameters during wave periods (red line) and all solar wind periods (blue line). The vertical dashed lines indicate the median values. The right column shows the relative occurrence rates (black line) by normalizing the occurrence time of each parameter during the storm event over the total solar wind interval for that parameter in 2008. A comparison with all solar wind periods suggests that the storm events tend to occur when the angle between the magnetic field direction and the radial direction from the Sun (i.e., B–R acute angle) is small. In Figure 15.4a, the B–R acute angle during wave

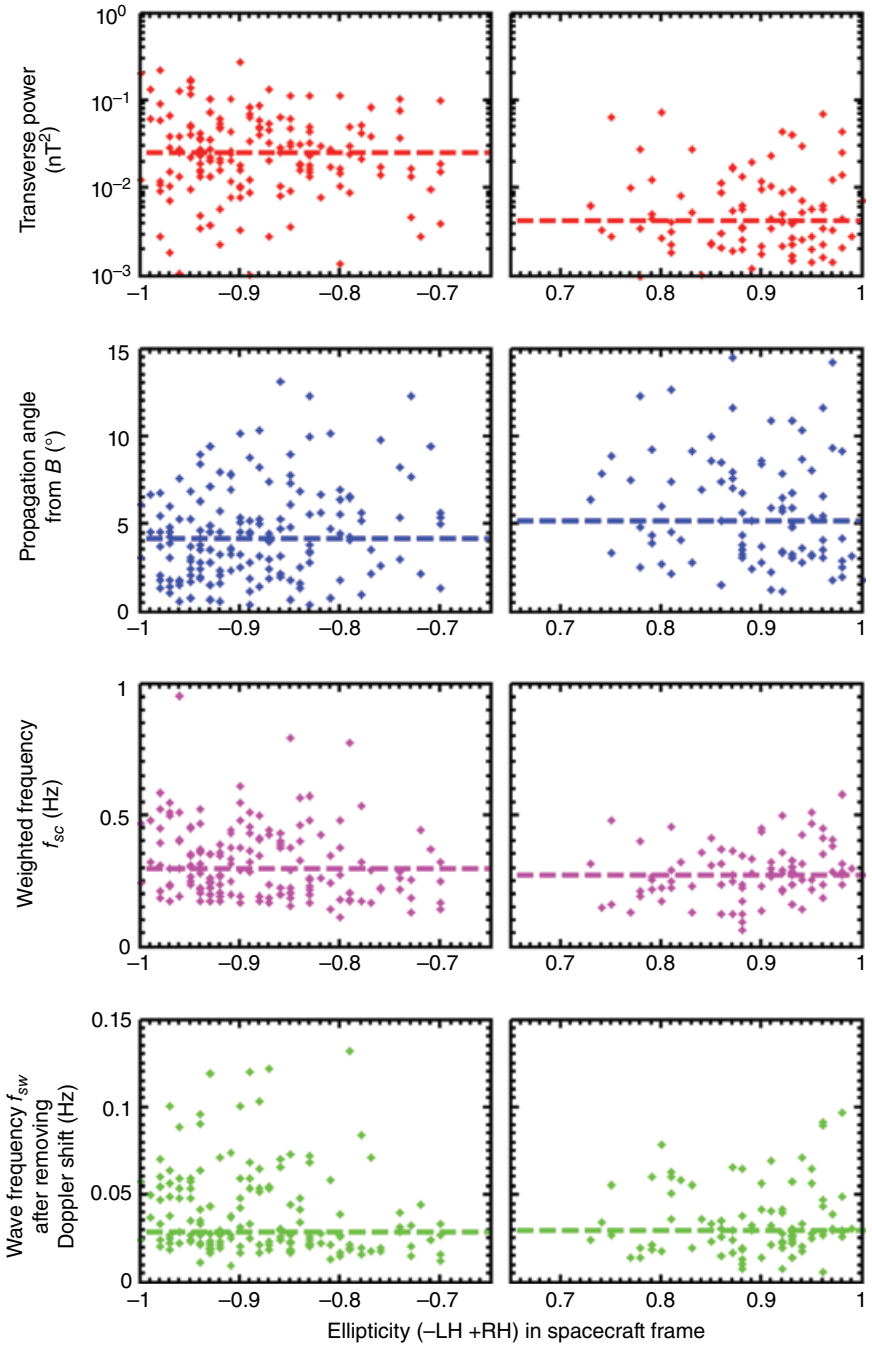

Figure 15.3 Comparison of the wave parameters of LH and RH waves in spacecraft frame. The dashed lines in each panel show the corresponding median values [*Jian et al.,* 2009].

storms is mainly distributed between 6° and 36°, while the angle during all solar wind periods is mainly distributed greater than 30°. For other solar wind parameters, the differences between wave intervals and all solar wind periods are small, with the wave-storm periods having slightly slower solar wind velocity, smaller proton density, cooler proton temperature, and lower β (with β being the ratio of plasma pressure over magnetic pressure). Although the waves tend to occur during radial field geometry, not all radial field intervals contain detectable waves. *Jian et al.* [2014] suggest that this may be due to the waves being generated remotely and the solar wind field directions being constantly changing or due to some additional solar wind conditions needing to be satisfied for the waves to grow.

Ion–beam distributions, such as proton double streams or proton-α particle differential streams, may also

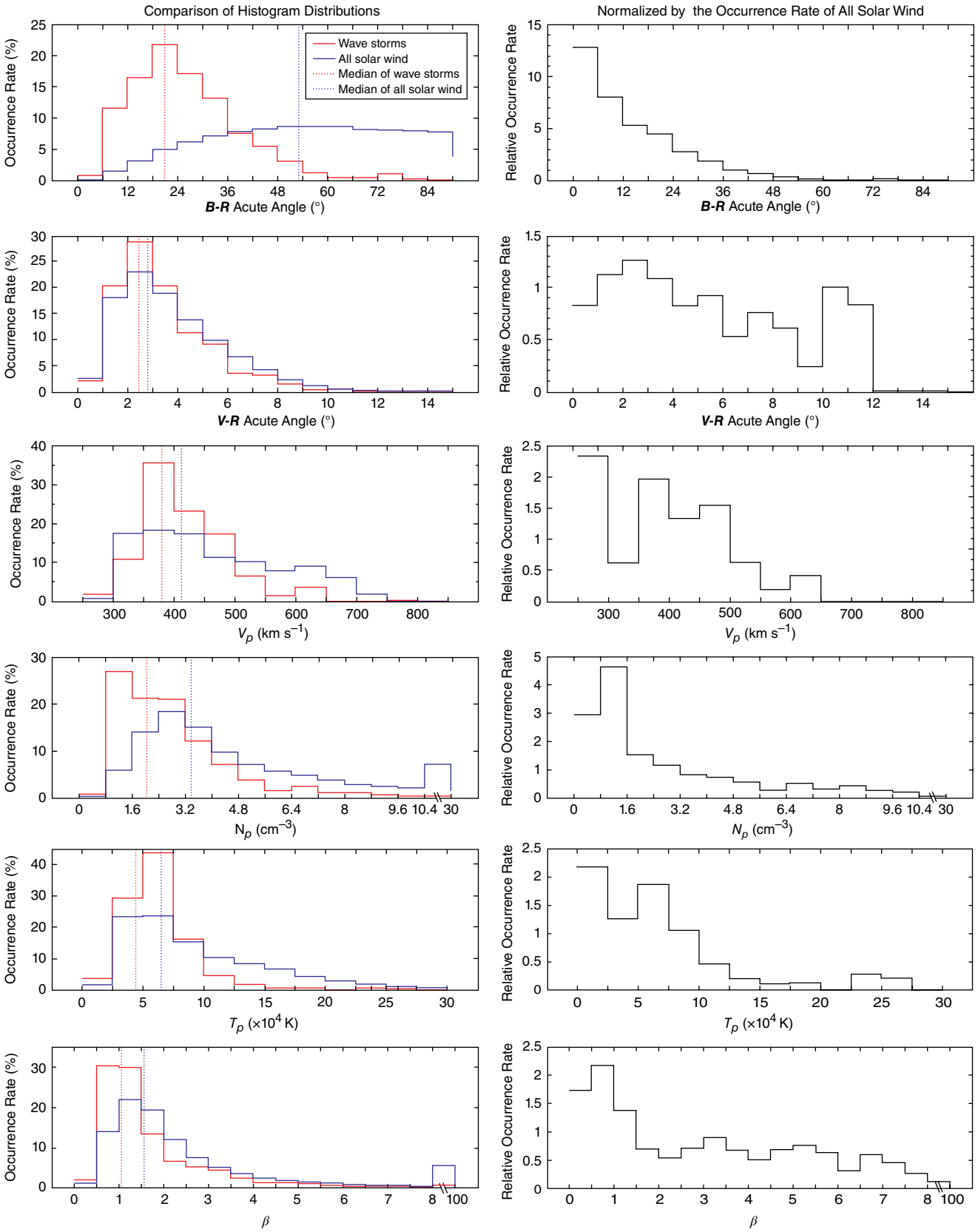

Figure 15.4 (left) Histogram comparison of solar wind parameters between wave-storm periods (red lines) and all solar wind in 2008 (blue lines). (right) Relative occurrence rate of the parameter in wave storms normalized by the rate in all solar wind [*Jian et al.*, 2014].

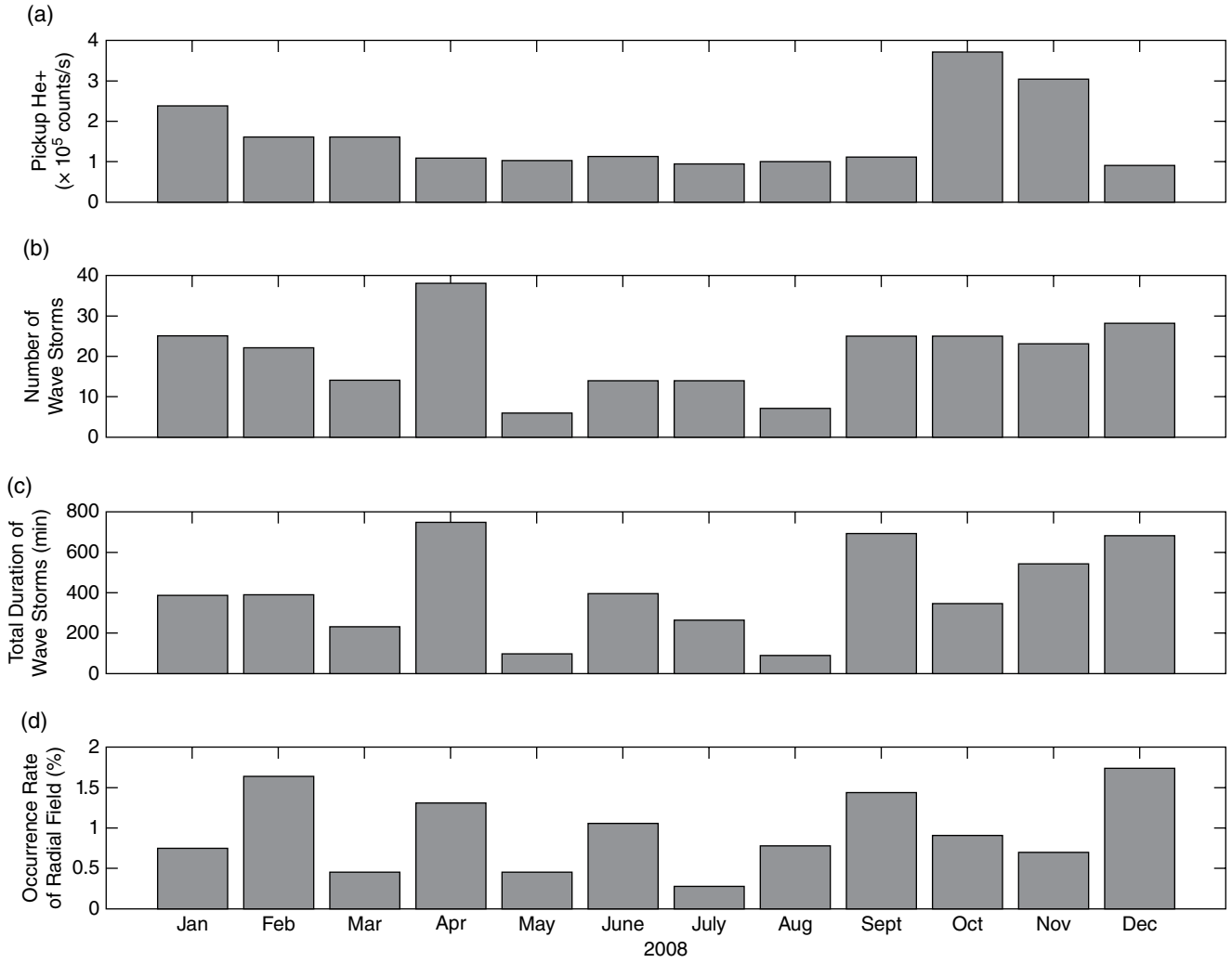

Figure 15.5 Monthly distributions of the flux of interstellar pickup He^+ (a), the occurrence number of storm events (b), the cumulative duration of the storm events (c), and the fractional occurrence rate (d) of radial field (B–R acute angle <10°) in 2008 [*Jian et al.*, 2014].

contribute to the wave generation by creating right-handed magnetosonic waves or by changing the resonant condition for wave-particle interactions. Since proton beam distribution functions were not available from STEREO data, *Jian et al*. [2014] examined the relative solar wind parameters of α-particles to protons during the storm-event intervals. They found that, in contrast with the general solar wind, the storm events had a faster differential flow between α-particles and protons normalized by Alfvén speed ($|V\alpha - Vp|/V_A$), a higher density abundance ratio between α-particles and protons ($N\alpha/Np$), and a higher temperature ratio between α-particles and protons ($T\alpha/Tp$), as might suggest that the storm events are related to α beams. However, *Jian et al*. [2014] also argue that the significance of this correlation could be compromised by the limitation of the one-dimensional Maxwellian fit used to calculate the moments for protons and α-particles, so further confirmation would be required using another data set built on two-dimensional fits.

Another possible wave generation mechanism is associated with the pickup ions. The pickup ions at STEREO-A spacecraft can originate from interstellar neutral gas, the inner heliosphere including the solar corona, or cometary nuclei. For the interstellar neutral species heavier than atomic hydrogen, the solar gravitation is greater than radiation pressure, so the neutral gas is focused on the downwind side of the Sun relative to the interstellar medium, called the focusing cone [*Fahr*, 1974]. To examine if the interstellar pickup ions are responsible for wave storms, *Jian et al*. [2014] performed correlation studies on

the storm event occurrence rate and the count rate of interstellar pickup He^+ (which is used to represent both interstellar pickup Ne^+ and He^+ because they have the same focusing cone [*Drews et al*., 2010]). The focusing cone of He^+ observed by STEREO-A was in October and November 2008, as shown in Figure 15.5a. For both monthly event number (Figure 15.5b) and monthly accumulative duration (Figure 15.5c) of wave storms, the three highest months are April, December, and September, all of which are outside the focusing cone. The correlation coefficients between the monthly pickup He^+ flux and the monthly storm event number, the monthly cumulative wave storm duration, and monthly average of wave transverse power are only 0.25, 0.0068, and 0.19, respectively. Thus *Jian et al*. [2014] suggest that the storm events are unlikely to be generated by interstellar pickup He^+ or Ne^+. Figure 15.5d shows the monthly fraction of time when the interplanetary magnetic field is in radial direction, which is quantified by the B–R acute angle smaller than 10°. The monthly storm-event occurrence (in Figures 15.5b and 15.5c) is well correlated with the occurrence of radial interplanetary field (in Figure 15.5d), with a correlation coefficient of 0.71. This correlation is also observed for the short-duration events, suggesting the radial field geometry is a universal condition for either generating or sustaining these waves.

So far these ICWs have been observed over all longitudes of the Sun. The sources of the waves are unlikely to be ICMEs, interplanetary shock, solar energetic particles, comets, planetary exospheres, and interplanetary pickup ions. It remains a mystery how these waves are generated, and high-quality plasma data are required during the wave intervals to determine whether they are generated locally or remotely. Because the solar wind velocity is typically much faster than the wave group velocity, the waves can hardly propagate inward to the Sun; thus the question is how far inside the spacecraft's distance were they generated and how much have the waves evolved or damped from their source region to the spacecraft location. Understanding the energy sources of these waves and their effects to the solar wind (e.g., heating and acceleration) could provide important information on the physical process in the collisionless solar wind plasma in the inner heliosphere.

15.4. GENERATION OF ICWS IN THE SOLAR WIND BY TEMPERATURE ANISOTROPY INSTABILITY

One promising wave generation source that still remains open is the pickup ions or ion species with high-temperature anisotropy in the inner heliosphere including the solar corona. If so, these waves may reveal important information regarding the role they play in solar wind heating in the inner heliosphere and the solar corona [e.g., *Isenberg and Vasquez*, 2011; *Omidi et al*., 2014a]. The source of the instability is the cyclotron resonance of the waves with ion velocity distribution functions that have a temperature perpendicular to the magnetic field larger than parallel, the so-called ion cyclotron temperature anisotropy instability [e.g., *Gary et al*., 1984; *Gary*, 1993]. Observations show that in the coronal holes and the acceleration region of the fast solar wind, ions are more heated in the direction perpendicular to the magnetic field than in the parallel direction [e.g., *Kohl et al*., 1988; *Dodero et al*., 1998; *Antonucci et al*., 2000; *Cranmer et al*., 2008]. Furthermore, these observations show that each ion species develops its own temperature and level of temperature anisotropy (i.e., the ratio of perpendicular temperature to parallel temperature) due to the lack of collisions, and both the temperature and the value of anisotropy increase with the mass of the ion species. The solar wind protons are also found to maintain some level of temperature anisotropy to the distance of 1 AU despite the perpendicular cooling effect during solar wind expansion [e.g., *Marsch et al*., 2004; *Hellinger et al*., 2011]. Thus *Omidi et al*. [2014a, b] argued that the generation and absorption of ion cyclotron waves may be ongoing in the corona and solar wind, regulating plasma temperature and the level of anisotropy.

With the objective of understanding the generation, propagation, and nonlinear evolution of ICWs in the corona and the solar wind, hybrid simulations are performed under a wide range of plasma conditions relevant to the corona and solar wind for uniform and nonuniform magnetic field background [*Omidi et al*., 2014a, b]. The hybrid model, which treats ions kinetically as macroparticles and electrons as a massless fluid, has two dimensions in space and three dimensions in velocity and electromagnetic fields. The model consists of protons as the sole or majority species, with either He^{2+} or O^{5+} as the minor ion species, which have velocity distributions as Maxwellian, bi-Maxwellian, or Fermi-accelerated distributions. The bi-Maxwellian distribution allows the ions to have different perpendicular temperature (T_{perp}) and parallel temperature (T_{para}) regarding the magnetic field direction. The Fermi-accelerated distribution is reported by *Isenberg et al*. [2010] for O^{5+} ions, which has larger perpendicular temperature than parallel temperature due to the second-order Fermi acceleration in the corona through wave-particle interaction with Sunward and anti-Sunward propagating ion cyclotron waves.

A range of ion densities, temperature anisotropy levels (i.e., T_{perp}/T_{para}), and ion β were simulated, and showed that ion cyclotron waves can be generated under a wide range of

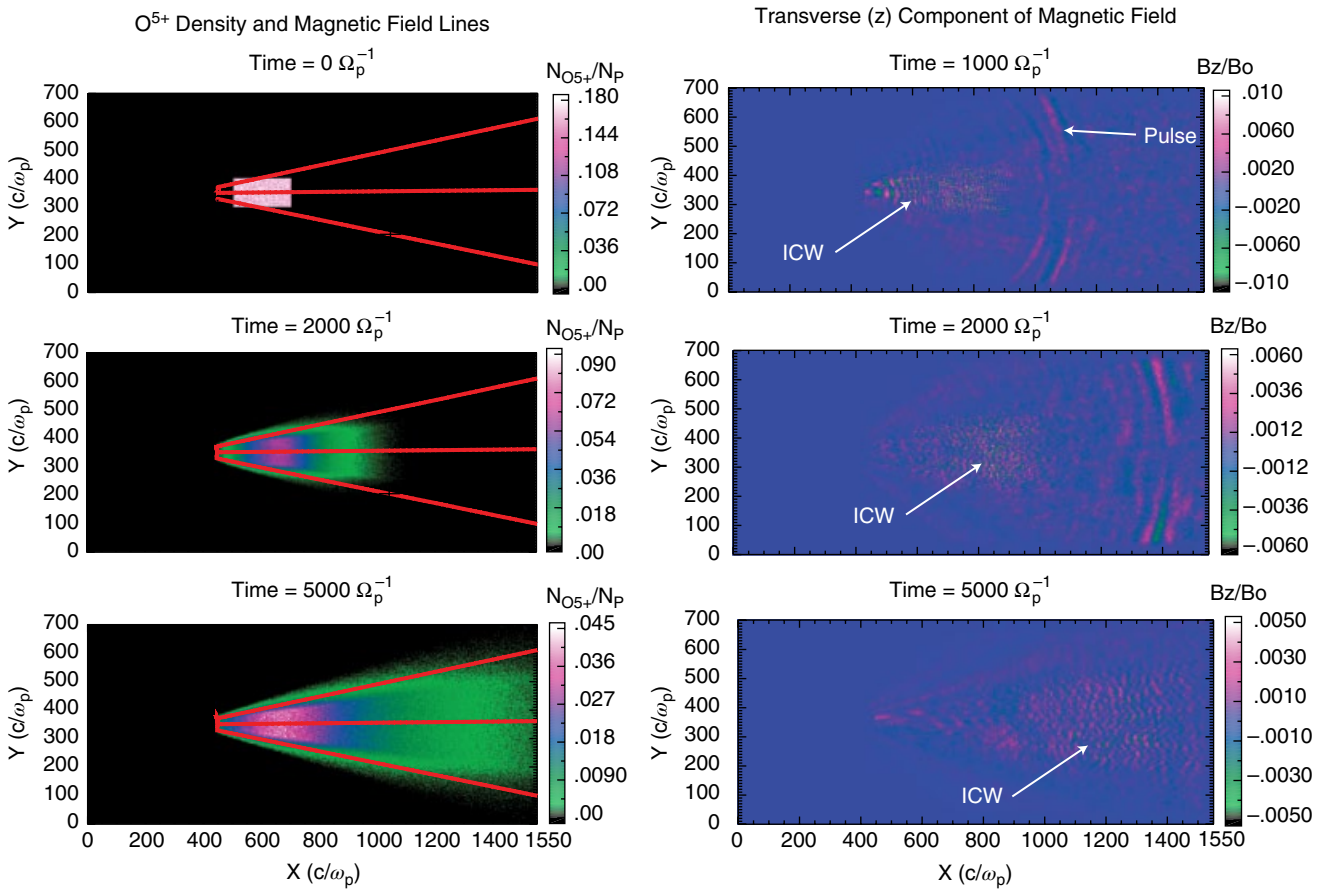

Figure 15.6 Evolution of the O^{5+} ions (in left three panels) and of the ICWs (in right three panels) with simulation time [*Omidi et al.*, 2014b].

plasma conditions for uniform magnetic field background. In particular, the effects of these parameters are as follows: (1) in a proton–electron plasma, when ion β exceeds a certain level, ion temperature anisotropy can generate ICWs that propagate parallel and anti-parallel to the magnetic field, and the wave saturation amplitude increases with ion β; (2) the addition of minor ion species leads to a branch associated with the minor ions with frequencies below the gyro-frequency of these ions, besides a proton branch with frequencies between the gyro-frequencies of the minor ions and protons; (3) the general properties of the instability and the nonlinear evolution of the waves are not sensitive to the details of the velocity distribution functions (i.e., bi-Maxwellian and Fermi-accelerated distributions lead to similar results); (4) when there are relative drifts between the protons and minor ions, oblique ion cyclotron waves are generated when using Fermi-accelerated distribution functions but not when using bi-Maxwellian distribution functions [*Omidi et al.*, 2014a].

To examine the effects of nonuniform magnetic field strengths and geometries, simulations are carried out for stationary uniform thermal background plasma (with protons and electrons) and radial and spiral field geometries with field strength dropping linearly or quadratically with radial distance [*Omidi et al.*, 2014b]. The energy source of ICWs is minority O^{5+} ions with a Fermi-accelerated velocity distribution. Figure 15.6 shows the evolution of the O^{5+} ions (left three panels) and of the ICWs (right three panels) with simulation time. The O^{5+} ions expand along field lines with time due to their thermal velocity parallel to the magnetic field, and they are removed once reaching the outer boundary. The short wavelength waves labeled ICW are circularly polarized ion cyclotron waves generated by the temperature anisotropy of O^{5+} ions which propagate primarily parallel and anti-parallel to the magnetic field. Ahead of these waves is a fast magnetosonic pulse generated by the pressure perturbations associated with the initial presence of O^{5+} ions that propagates out of the system.

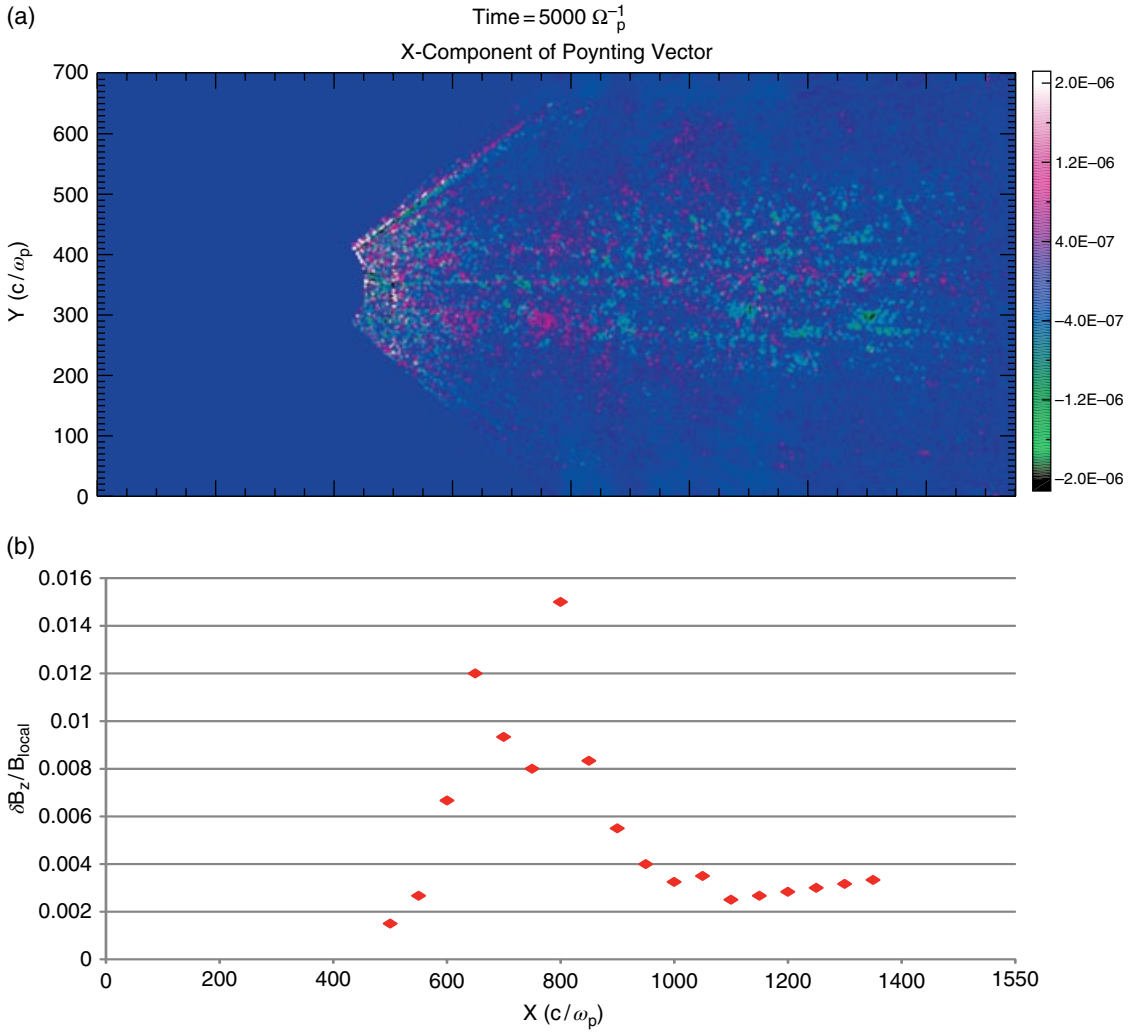

Figure 15.7 (a) **X** component of the Poynting vector showing ICWs propagating parallel (magenta and white) and antiparallel (green and black) to the magnetic field. (b) Amplitude of ICWs as a function of radial distance normalized to the local magnetic field strength [*Omidi et al.*, 2014].

By examining the ICWs at different radial distances, *Omidi et al.* [2014b] demonstrated that the wave generation and absorption take place at all radial distances as the O^{5+} ions expand outward, because the waves at different distances are below the local ion gyro-frequencies. Figure 15.7 shows the X-component of the Poynting vector (Figure 15.6a) and the normalized ICW amplitude (Figure 15.6b). Positive values (magenta and white colors) of the Poynting vector imply group velocity along the +X direction, while negative values (green and black colors) correspond to group velocity along the −X direction. Both outward and inward propagating waves are present at all radial distances, indicating that the waves are generated locally rather than at a smaller radial distance (i.e., the initial source region) and propagating outward. The radial variation of the wave amplitude is interpreted due to the change in the properties of O^{5+} ions as they expand and interact with the waves. The simulations for both radial and spiral magnetic fields show similar wave generation and propagation along the field lines, possibly due to the lack of background plasma velocity and density gradients in the simulation [*Omidi et al.*, 2014b]. Future work is required to include more realistic solar wind conditions for investigating the wave propagation, evolution, and absorption as they are carried out of the source region.

15.5. THE WAVE SOURCE REGION IMPLIED FROM LH AND RH WAVE OBSERVATIONS

To better understand the wave source region, case studies have been performed on a special group of ICW storm events, in which the left-handed (LH) and right-handed (RH) waves were observed simultaneously in the spacecraft frame. The study in this section assumes the waves are generated through one possible mechanism (i.e., the temperature anisotropy instability), as investigated in Section 15.4; however, there are other possible mechanisms to study in future works.

Figure 15.8 shows such an event that was observed on September 14, 2008, by the STEREO-A spacecraft at a radial distance of 0.96 AU and an azimuthal angle of 39° from the Earth. Figure 15.8 (top panel) shows the dynamic spectrum of the transverse power, which has two wave bands from 0000 to 0305 UT with the upper band near 0.15 Hz and the lower band near 0.07 Hz. Figure 15.8 (middle panel) shows the ellipticity of these waves, with the upper band being left-handed polarized and the lower band being right-handed polarized. Figure 15.8 (bottom panel) shows the wave propagation angle, whereby both LH and RH waves propagate nearly parallel to the magnetic field. Wave analysis by the *Means* [1972] method on the interval between 0025 to 0030 UT shows that the RH wave has a frequency of 0.068 Hz, an ellipticity of 0.801, and a propagation angle of 6°, while the LH wave has a frequency of 0.138 Hz, an ellipticity of −0.878 and a propagation angle of 2°. Although the statistical study of *Jian et al.* [2014] shows that the storm events are observed about 0.9% of time in 2008 by STEREO-A, these events usually only observed either LH or RH waves. The simultaneous observations of both LH and RH waves are much less frequent. If these waves are generated close to the Sun by pickup ion or ion species with large temperature anisotropy, the LH waves should travel to the spacecraft location within shorter time than the RH waves. The different propagation times between LH and RH waves should separate them in the time domain at the spacecraft location, except if the waves are generated by a source that continuously produces the waves for a longer time than the propagation time difference. For the storm events it is likely that the wave source has been generating the waves over a long time.

If these simultaneously observed LH and RH waves were generated by the same source remotely in the inner heliosphere, the wave properties observed at STEREO-A could be used to estimate their Doppler-shift frequencies and also the location of the source region. The underlined assumption is that if a virtual spacecraft were placed at the source region, it would observe the same wave properties and wave frequencies of LH and RH waves (in the spacecraft frame) as STEREO near 1 AU. This is likely because if nearly radial magnetic field geometry is assumed from the source region to the spacecraft, the wave property and frequency should not change much as they propagate and are carried out from the Sun, as long as the wave frequency has not reached the local proton gyro-frequency and thus has not suffered much damping. Based on the simulation results from *Omidi et al.* [2014b],

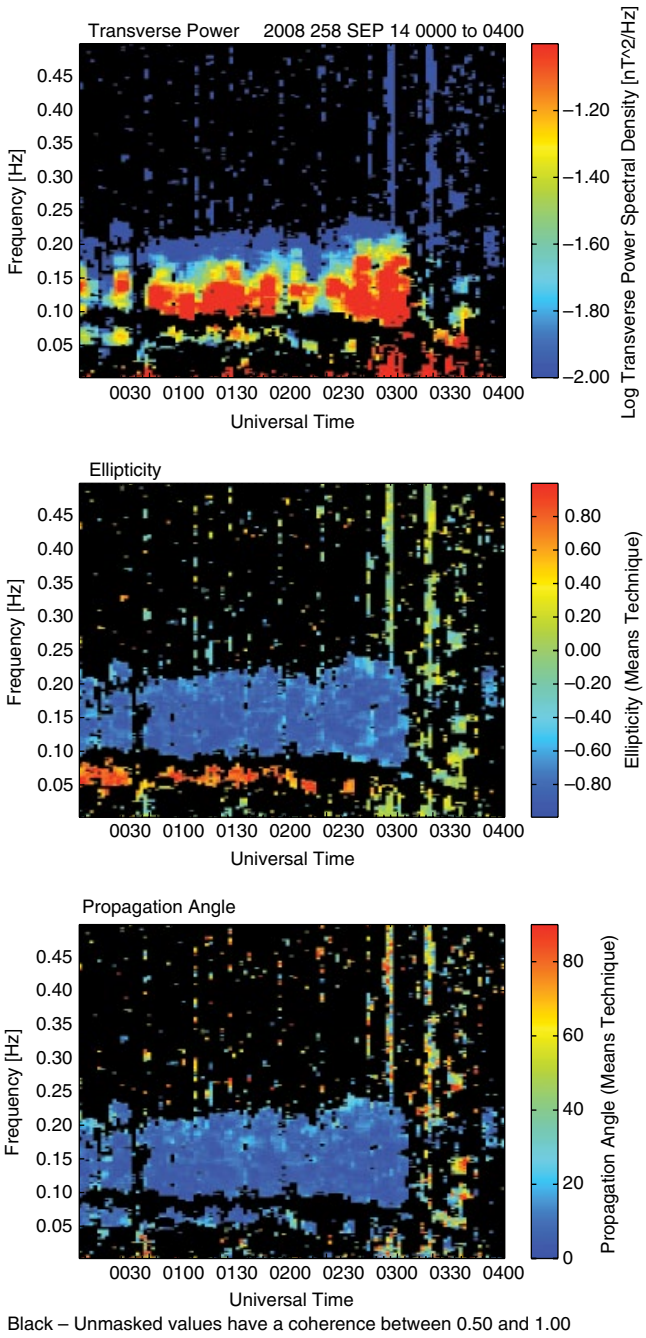

Figure 15.8 Dynamic spectra of transverse power (top), ellipticity (middle), and propagation angle (bottom) for wave-storm events with simultaneous LH and RH waves. Only values with coherence between B_T and B_N greater than 0.5 are shown.

the two following assumptions are also reasonable: the wave frequencies in the plasma frame of the source solar wind are the local gyro-frequency of the source ion species (with moderate temperature anisotropy that is also large enough for ICW generation), and the wave phase speed (ω/k) is the Alfvén velocity in the source solar wind frame. Thus, for the Sunward-propagating wave (i.e., the RH wave), $f_R = f_{ssw} + \frac{\overrightarrow{k_R} \cdot \vec{V}_{SSW}}{2\pi}$, and for the anti-Sunward-propagating wave (i.e., the LH wave), $f_L = f_{ssw} + \frac{\overrightarrow{k_L} \cdot \vec{V}_{SSW}}{2\pi}$, where f_L, f_R, f_{ssw}, and $\vec{V}_{SSW}$ are the wave frequencies in the spacecraft frame for LH and RH waves, the wave frequency in the source solar wind frame, and the source solar wind velocity, respectively. After using the Alfvén velocity at the source region (V_A) to approximate the wave phase speed (ω/k), these two equations can be written as $|f_R| \approx f_{ssw}\left[\frac{V_{ssw}}{V_A}\cos(\theta_R) - 1\right]$ and $f_L \approx f_{ssw}\left[1 + \frac{V_{ssw}}{V_A}\cos(\theta_L)\right]$, where θ_R and θ_L are the acute angle between the wave vector (obtained from wave analysis) and the solar wind velocity (assumed to be radial). Thus the wave frequency in the plasma frame of the source region can be obtained as $f_{ssw} = \frac{f_L \times cos\theta_R - |f_R| \times cos\theta_L}{cos\theta_L + cos\theta_R}$, which can be approximated as the source ion gyro-frequency. Assuming the source ion species has a certain mass to charge ratio $\left(\frac{m}{q}\right)$, the magnetic field strength at the source region can be obtained as $B_{source} = 2\pi \times \frac{m}{q} \times f_{SSW}$. Because the magnetic field is nearly radial when these ICWs are observed, the field strength can be approximated as decreasing quadratically with heliocentric distance. Thus the location of the source region (R_{source}) can be obtained as $R_{source} = R_{s/c} \times \sqrt{B_{s/c} / B_{source}}$, where $R_{s/c}$ and $B_{s/c}$ are the heliocentric distance and observed magnetic field at the spacecraft. The solar wind velocity at the source region can also be obtained as $V_{ssw} = \frac{f_L + |f_R|}{cos\theta_L + cos\theta_R} \times \frac{V_A}{f_{ssw}}$, where V_A is the Alfvén speed at the source region and can be obtained by assuming both the magnetic field strength and the plasma density decrease quadratically with distance from the Sun (i.e., $V_A = 21.8\sqrt{B_{source} B_{s/c} / \rho_{s/c}}$ in unit of km/s), where $\rho_{s/c}$ is the plasma density at the spacecraft. From the properties of the waves between 0025 to 0030 UT in Figure 15.8, the estimated f_{ssw} is 0.036 Hz, which leads to B_{source} of 7.6 nT if assuming O^{5+} as the source ion species. Since the field strength at the spacecraft is 2.4 nT, the estimated source location (R_{source}) is 0.56 AU, and the source solar wind speed is 195 km/s.

The preceding analysis is applied to all the storm events with coexisting LH and RH waves to estimate the source locations and source solar wind properties. From 2008 STEREO A data, there were 24 storm events with coexisting LH and RH waves, and wave analysis was applied to 36 intervals among them. The durations of these 36 intervals are from 2 to 10 min with an average of 4 min. These events were picked by eye to ensure significant wave powers of both LH and RH waves. There are two or three intervals selected in some of the storm events. For example, in the event in Figure 15.8, two intervals are selected (i.e., 0025–0030 UT and 0125–0135 UT). For such situations, the selected intervals are at least 10 minutes apart and usually over an hour apart. Figure 15.9 shows the estimated solar wind velocity at the source region versus the solar wind velocity (left panel) at the spacecraft location, and versus the Alfvén speed (right panel) at the source region, for O^{5+} ions. The estimated ratios of V_{SSW} and local solar wind speed are mostly smaller than 1 and have a median of 0.34. The ratios of V_{SSW} and the Alfvén speed at source region are between 1.3 and 5.2, with a median of 3.0. These values are in agreement with the assumption that the RH waves are intrinsically left-handed in plasma frame at the source region, but the Doppler shift is greater than the wave frequency so that they become right-handed in the spacecraft frame.

Both the heliocentric distance of the source region and the solar wind speed at the source region are dependent on the assumptions of the ion species generating these ICWs. Thus these two parameters are calculated based on assumptions of some typical solar wind ion species, H^+, He^{2+}, O^{5+}, Fe^{9+} (Figure 15.10). The wave phase speed is slower than the solar wind speed (to make RH waves in the spacecraft frame), so the source location should be inside 1 AU. Clearly, the waves are unlikely to be generated by H^+ because over half the waves would be generated outside 1 AU. If the solar wind is generally accelerating rather than decelerating, Fe^{9+} or ions with greater mass-to-charge ratios would unlikely be responsible for these waves. From these two constraints, the possible ion species to generate these ICWs should have a mass-to-charge ratio of about 2 to 4, corresponding to a series of heavy ions from the solar corona. Even heavier ions may become possible candidates if the waves occur in the decelerating solar wind. Moreover, although we assume the waves in the source solar wind frame are near the pickup ions' gyro-frequencies, as predicted by linear theory of dispersion relation under an ideal situation, the simulation results of *Omidi et al.* [2014a, b] show peak powers at frequencies from right below to 30% of pickup ion gyro-frequency (see Figure 8 of *Omidi et al.* [2014a] and Figures 5 and 7 of *Omidi et al.* [2014b]). If we choose 30% of gyro-frequency in our assumption instead of the full gyro-frequency, the source distance would reduce by

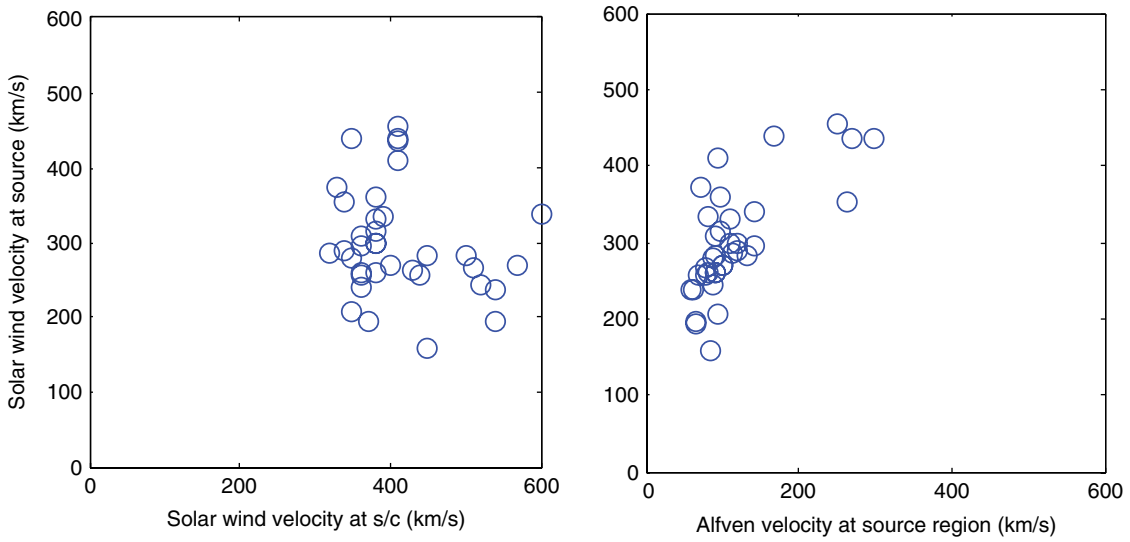

Figure 15.9 Estimated solar wind velocity at the source region compared with solar wind velocity (left) at the spacecraft and with the Alfvén velocity (right) at the source region for O^{5+} ions.

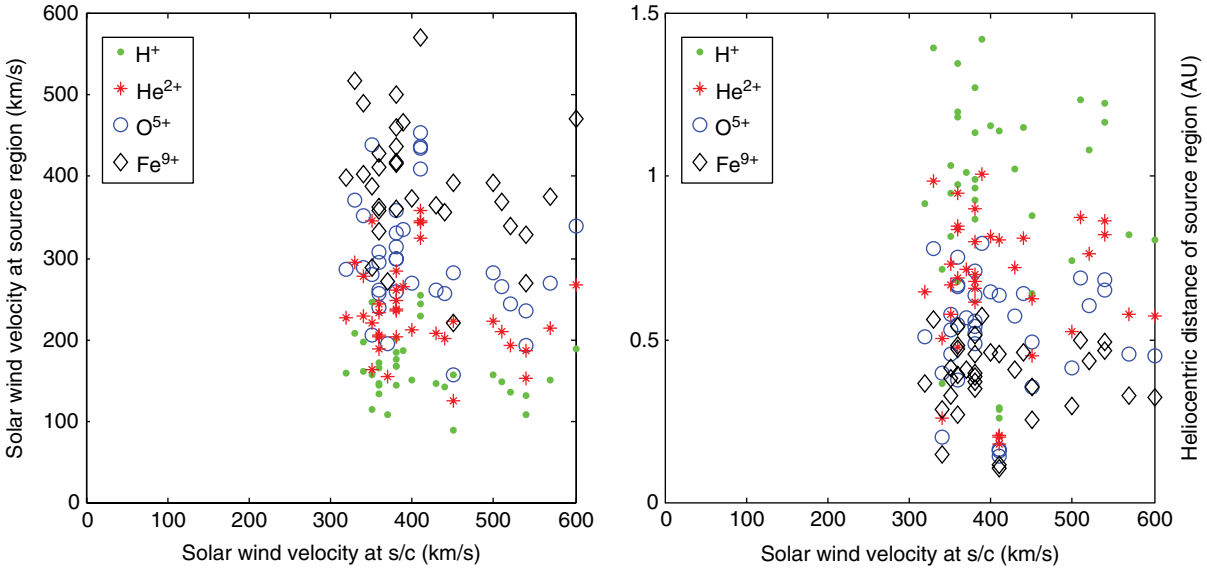

Figure 15.10 Estimated solar wind velocity (left) and the heliocentric distance (right) of the source region, based on assumptions of some typical solar wind ion species, H^+, He^{2+}, O^{5+}, Fe^{9+}.

a factor of 0.58 and the source solar wind velocity would increase by a factor of 1.73. This extreme situation would allow the source location of protons within 1 AU, which would not exclude them as possible source ions.

15.6. VARIATIONS OF ICW PROPERTIES WITH HELIOCENTRIC DISTANCE FROM 0.3 TO 1 AU

The variations of the wave properties with heliocentric distances may also provide information on the possible wave generation sources and the effects of the wave to the solar wind plasma. Figure 15.11 shows the comparison of LH and RH wave properties at 0.3, 0.7, and 1 AU. The panels in the first row show the wave power trace (which is the sum of power in the three components of the magnetic field). Because these waves are highly transverse waves, the power trace is nearly equal to the transverse power. It is noticeable that the wave power is significantly stronger at 0.3 AU than at 0.7 and 1 AU. The wave propagation angle is mostly within 10° for all three distances and shows few differences (panels in the second row of Figure 15.11). The panels in the third row show the wave

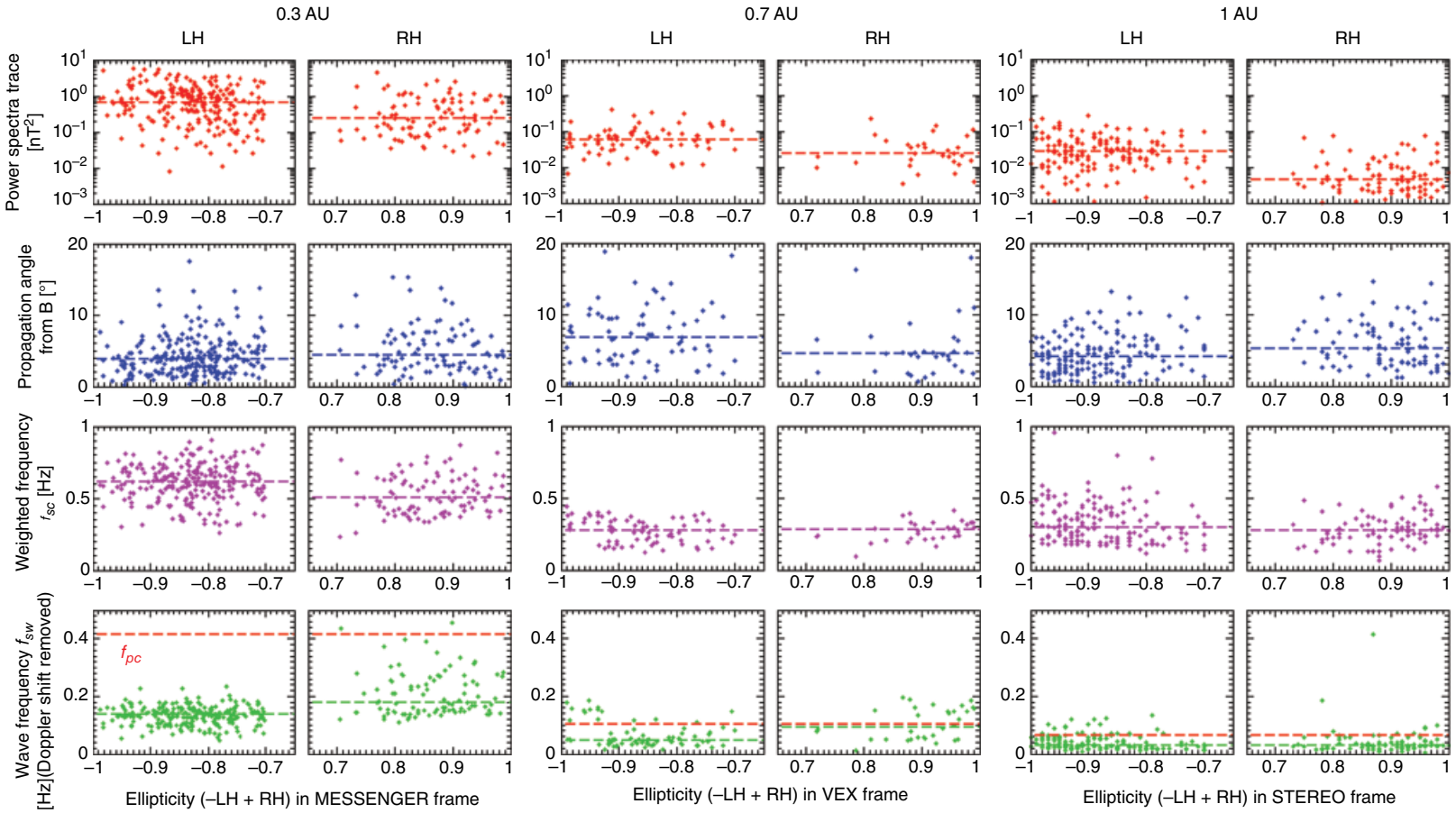

Figure 15.11 Variation of ICW properties over three heliocentric distances. All events are selected with the same criteria in *Jian et al*. [2009, 2010, 2014], with observations from MESSENGER, Helios-1, Venus Express, and STEREO. The observations at 0.7 AU are obtained 4 hours around the apoapsis to minimize the influence from Venus's interaction with the solar wind. The dashed line in each panel indicates the corresponding median value except for the red line in the bottom panels marking local proton gyro-frequency.

frequencies in the spacecraft frame, and the frequency is significantly higher at 0.3 AU than at 0.7 and 1 AU. The panels in the last row show the wave frequency in the plasma frame of the local solar wind. They are mostly below the local proton gyro-frequency, in agreement with the fact that they have not experienced severe damping.

The decrease of wave amplitude with distance supports the hypothesis that many (not necessarily all) waves are generated in the inner heliosphere (less than 0.3 AU) and that they propagate and are carried out with the solar wind. In this scenario, the waves could be generated over a large range of frequencies, and the waves get absorbed by the local plasma when their frequencies reach the local proton frequency in the solar wind. It is also possible that the waves have a wide bandwidth in frequency and that the high-frequency portion gets eroded gradually as the waves propagate and convect out in the solar wind. The wave powers of LH waves are stronger than the powers of RH waves for all three heliocentric distances. This can be interpreted as the LH waves (which propagate anti-Sunward) experiencing less damping than the RH waves (which propagate Sunward) when reaching the spacecraft downstream of the wave source region [*Jian et al*., 2009]. The decrease of the wave frequency with distance may support the idea that the waves generated more locally or just slightly upstream of the spacecraft location. However, the decrease of the wave frequency can also be caused by the gradual erosion of the wave power spectra in the high-frequency portion, as the local solar wind proton frequency decreases when waves propagate and convect outward in the solar wind. The bandwidth and shape of the wave power spectra need to be studied in more detail in future work.

15.7. CONCLUSIONS AND DISCUSSIONS

Parallel propagating and circularly polarized transverse electromagnetic waves near the proton gyro-frequency are observed in the inner heliosphere far from planetary or cometary sources. To understand the wave properties, energy sources, and effects on the solar wind plasma, observational and simulation studies are performed. The results obtained so far are as follows.

1. The wave properties are similar in storm events and short-duration events. The waves may be generated frequently in the inner heliosphere and gradually damped as they propagate and convect outward with the solar wind, or there could be a continuous generation of waves.
2. The wave frequencies decrease with heliocentric distances, and are generally below the local proton gyro-frequency in the plasma frame of the solar wind, in agreement with the wave power having not suffered severe damping by the background thermal plasma.
3. The waves are observed to be either left-handed or right-handed in the spacecraft frame, but they could be just left-handed in the plasma frame of the solar wind. The left-handed waves are observed more often and have higher median amplitude than the right-handed waves for all three heliocentric distances.
4. The wave occurrence rates are enhanced when the solar wind magnetic field is in nearly radial geometry, which could be due to the wave damping being minimized for such geometry.
5. The majority of the waves are observed far away from planetary or cometary sources when there are no ICMEs, shocks, flares, and solar energetic particle events, and there is little correlation between the wave occurrence rate and the flux of interstellar pickup He^+ and Ne^+. Thus they are unlikely to be the sources for these waves.
6. Hybrid simulations on relatively idealized solar wind conditions show that parallel and anti-parallel propagating waves can be generated by the free energy of ion species with temperature anisotropy, under a wide range of plasma conditions relevant to the corona and solar wind for uniform and nonuniform magnetic field background. The simulation results agree with observations qualitatively, but it requires future work to simulate the wave evolution under more realistic solar wind conditions.
7. With idealized assumptions, case studies on a special group of events with simultaneous left-hand and right-hand waves suggest that wave source region can be much closer than 0.3 AU, and the ion species generating the wave possibly have mass-to-charge ratios of about 2 to 4.
8. Although several wave properties are in agreement with remote generation sources, it requires future studies on the plasma data to examine the possibility of local generation.

ACKNOWLEDGMENTS

These works were supported by NASA grants NNX12AB29G, NNX13AI65G, NNX11AJ37G, NNX13AF97G, and NNX15AB75G, by NSF SHINE grant AGS0962506, and by NASA's STEREO program through grant NASS-03131 administered by UC Berkeley.

REFERENCES

Antonucci, E., M. Dodero, and S. Giordano (2000), Fast solar wind velocity in a polar coronal hole during solar minimum, *Sol. Phys.*, *197*, 115–134.

Cranmer, S. R., A. V. Panasyuk, and J. L. Kohl (2008), Improved constraints on the preferential heating and acceleration of oxygen ions in the extended solar corona, *Astrophys. J.*, *678*, 1480–1497.

Dodero, M., E. Antonucci, S. Giardano, and R. Martin (1998), Solar wind velocity and anisotropic coronal kinetic temperature measured with the O VI doublet ratio, *Sol. Phys.*, *183*, 77–90.

Drews, C., L. Berger, R. F. Wimmer-Schweingruber, A. B. Galvin, B. Klecker, and E. Möbius (2010), Observations of interstellar neon in the helium focusing cone, *J. Geophys. Res.*, *115*, A10108, doi:10.1029/2010JA015585.

Gary, S. P. (1993), *Theory of Space Plasma Microinstabilities*, Cambridge Univ. Press, New York.

Gary, S.P., C. W. Smith, M. A. Lee, M. L. Goldstein, and D. W. Fooslund (1984), Electromagnetic ion-beam instabilities, *Phys. Fluids*, *27*(7), 1852–1862.

Hellinger, P., L. Matteini, Š. Štverák, P. M. Trávníček, and E. Marsch (2011), Heating and cooling of protons in the fast solar wind between 0.3 and 1 AU: Helios revisited, *J. Geophys. Res.*, *116*, A09105, doi:10.1029/2011JA016674.

Isenberg, P. A., and B. J. Vasquez (2011), A kinetic model of solar wind generation by oblique ion-cyclotron waves, *Astrophys. J.*, *731*, 88.

Isenberg, P. A., B. J. Vasquez, and S. R. Cranmer (2010), Modeling the preferential acceleration and heating of coronal hole O5+ as measured by UVCS/SOHO, in *Solar Wind 12*, Vol. *1216* (eds. M. Maksimovic et al.), 56 pp., *AIP Conf. Proc*, Melville, NY.

Jian, L. K., C. T. Russell, J. G. Luhmann, R. J. Strangeway, J. S. Leisner, and A. B. Galvin (2009), Ion cyclotron waves in the solar wind observed by STEREO near 1 AU, *Astrophys. J.*, *701*, L105–L109, doi:10.1088/0004-637X/701/2/L105.

Jian, L. K., C. T. Russell, J. G. Luhmann, B. J. Anderson, S. A. Boardsen, R. J. Strangeway, M. M. Cowee, and A. Wennmacher (2010), Observations of ion cyclotron waves in the solar wind near 0.3 AU, *J. Geophys. Res.*, *115*, A12115, doi:10.1029/2010JA015737.

Jian, L. K., H. Y. Wei, C. T. Russell, J. G. Luhmann, B. Klecker, N. Omidi, P. A. Isenberg, M. L. Goldstein, A. Figueroa-Viñas, and X. Blanco-Cano (2014), Electromagnetic waves near the proton cyclotron frequency: STEREO observations, *Astrophys. J.*, *786*, 123, doi:10.1088/0004-637X/786/2/123.

Kohl, J. L., G. Noci, E. Antonucci, G. Tondello, M. C. E. Huber, S. R. Cranmer, L. Strachan, A. V. Panasyuk, L. D. Gardner, M. Romoli, S. Fineschi, D. Dobrzycka, J. C. Raymond, P. Nicolosi, O. H. W. Siegmund, D. Spadaro, C. Benna, A. Ciaravella, S. Giordano, S. R. Habbal, M. Karovska, X. Li, R. Martin, J. G. Michels, A. Modigliani, G. Naletto, R. H. O'neal, C. Pernechele, G. Poletto, P. L. Smith, R. M. Suleiman (1988), UVCS/SOHO empirical determinations of anisotropic velocity distributions in the solar corona, *Astrophys. J.*, *501*, L127–L131.

Marsch, E., X.-Z. Ao, and C.-Y. Tu (2004), On the temperature anisotropy of the core part of the proton velocity distribution function in the solar wind, *J. Geophys. Res.*, *109*, A04102, doi:10.1029/2003JA010330.

Means, J. D., (1972), Use of the three dimensional covariance matrix in analyzing the polarization properties of plane waves, *J. Geophys. Res. 77*(28), 5551–5559.

Omidi, N., P. Isenberg, C. T. Russell, L. K. Jian, and H. Y. Wei (2014a), Generation of ion cyclotron waves in the corona and solar wind, *J. Geophys. Res. Space Physics*, *119*, 1442–1454, doi:10.1002/2013JA019474.

Omidi, N., C. T. Russell, L. K. Jian, P. Isenberg, and H. Y. Wei (2014b), Generation and propagation of ion cyclotron waves in nonuniform magnetic field: Application to the corona and solar wind, *J. Geophys. Res. Space Physics*, *119*, 8750–8763, doi:10.1002/2014JA020315.